Organic Geochemistry 85 (2015) 42–53

Contents lists available at ScienceDirect

Organic Geochemistry

journal homepage: www.elsevier.com/locate/orggeochem

Rapid and simultaneous analysis of three molecular sea surface temperature proxies and application to sediments from the Sea of Marmara

Kevin W. Becker [a,*], Julius S. Lipp [a], Gerard J.M. Versteegh [b], Lars Wörmer [a], Kai-Uwe Hinrichs [a]

[a] Organic Geochemistry Group, MARUM Center for Marine Environmental Sciences & Dept. of Geosciences, University of Bremen, 28359 Bremen, Germany
[b] Heisenberg Group Marine Kerogen, MARUM Center for Marine Environmental Sciences & Dept. of Geosciences, University of Bremen, 28359 Bremen, Germany

ARTICLE INFO

Article history:
Received 16 December 2014
Received in revised form 21 April 2015
Accepted 28 April 2015
Available online 2 May 2015

Keywords:
HPLC–MS
Tetraether lipids
Long chain alkenones
Long chain diols
Sea surface temperature
$U^{K'}_{37}$
TEX_{86}
LDI
Sea of Marmara
Paleoclimate

ABSTRACT

Reconstructing ocean temperature values is a major target in paleoceanography and climate research. However, most temperature proxies are organism-based and thus suffer from an "ecological bias". Multiproxy approaches can potentially overcome this bias but typically require more investment in time and resources, while being susceptible to errors induced by sample preparation steps necessary before analysis. Three lipid-based temperature proxies are widely used: $U^{K'}_{37}$ (based on long chain alkenones from phytoplanktonic haptophytes), TEX_{86} [based on glycerol dialkyl glycerol tetraethers (GDGTs) from pelagic archaea] and LDI (based on long chain diols from phytoplanktonic eustigmatophytes). So far, separate analytical methods, including gas chromatography (GC) and liquid chromatography (LC), have been used to determine these proxies. Here we present a sensitive method for determining all three in a single normal phase high performance LC–atmospheric pressure chemical ionization mass spectrometry (NP-HPLC–APCI-MS) analysis. Each of the long chain alkenones and long chain diols was separated and unambiguously identified from the accurate masses and characteristic fragmentation during multiple stage MS analysis (MS^2). Comparison of conventional GC and HPLC–MS methods showed similar results for $U^{K'}_{37}$ and LDI, respectively, using diverse environmental samples and an *Emiliania huxleyi* culture. Including the three sea surface temperature (SST) proxies; the NP-HPLC–APCI-MS method in fact allows simultaneous determination of nine paleoenvironmental proxies. The extent to which the ecology of the source organisms (ecological bias) influences lipid composition and thereby the reconstructed temperature values was demonstrated by applying the new method to a sediment core from the Sea of Marmara, covering the last 21 kyr BP. Reconstructed SST values differed considerably between the proxies for the Last Glacial Maximum (LGM) and the period of Sapropel S1 formation at ca. 10 kyr BP, whereas the trends during the late Holocene were similar. Changes in the composition of alkenone-producing species at the transition from the LGM to the Bølling/Allerød (B/A) were inferred from unreasonably high $U^{K'}_{37}$-derived SST values (ca. 20 °C) during the LGM. We ascribe discrepancies between the reconstructed temperature records during S1 deposition to habitat change, e.g. a different depth due to changes in nutrient availability.

1. Introduction

Past ocean temperatures are an essential parameter for reconstructing the Earth's climate. Several organic and inorganic proxies for reconstructing sea surface temperature (SSTs) exist. Amongst these is the lipid based alkenone unsaturation index ($U^{K'}_{37}$), expressing the relative abundance of long chain alkenones biosynthesized by some haptophytes, in particular *Emiliania huxleyi* (Brassell et al., 1986), and the tetraether index with 86 carbon atoms (TEX_{86}), based on the relative abundance of isoprenoid glycerol dialkyl glycerol tetraethers (*i*GDGTs) biosynthesized by planktonic archaea (Schouten et al., 2002). Both proxies are widely used since they appear robust and applicable in most marine settings, and their analysis is inexpensive and requires only a small amount of sample < 1 g (e.g. Prahl et al., 1988; Müller et al., 1998; Schouten et al., 2002; Kim et al., 2008). More recently, the long chain diol index (LDI) has been proposed as an additional SST proxy (Rampen et al., 2012). It is based on the relative distribution of long chain diols, presumably produced by eustigmatophyte algae (Volkman et al., 1992; Versteegh et al., 1997). In paleoclimatology, a multiproxy approach is often used because each proxy has its limitations, such as alteration by selective

* Corresponding author. Tel.: +49 42121865715.
E-mail address: k.becker@uni-bremen.de (K.W. Becker).

http://dx.doi.org/10.1016/j.orggeochem.2015.04.008
0146-6380/

degradation and diagenesis (e.g. Hoefs et al., 1998; Schouten et al., 2004; Kim et al., 2009) or vulnerability to transport and redeposition (e.g. Ohkouchi et al., 2002; Mollenhauer et al., 2003). Additionally, the ecology of the different organisms and the resulting discrepancies between different SST proxies are not completely understood (e.g. Grauel et al., 2013; Smith et al., 2013; Lopes dos Santos et al., 2013). In order to minimize sources of errors and to allow high sample throughput in a relatively short time, simple and fast protocols are needed. At present, $U^{K'}_{37}$, LDI and TEX_{86} are obtained via separate analytical methods. $U^{K'}_{37}$ is conventionally obtained through gas chromatography (GC) coupled with either flame ionization detection (GC-FID) or mass spectrometry (GC–MS) operated in chemical ionization mode (CI; Rosell-Melé et al., 1995) or with fast GC–time-of-flight mass spectrometry (ToF-MS; Hefter, 2008). LDI is determined via GC–MS, while TEX_{86} is acquired using normal phase high performance liquid chromatography coupled to atmospheric pressure CI-MS (NP-HPLC–APCI-MS; Hopmans et al., 2000; Schouten et al., 2007). TEX_{86} can either be determined directly from the total lipid extract (TLE) or after fractionation over a silica gel or alumina column, whereas determination of $U^{K'}_{37}$ and LDI usually requires additional sample preparation steps, e.g. base hydrolysis to eliminate co-eluting alkenoates (Villanueva et al., 1997) or derivatization of hydroxyl groups of long chain diols. Other protocols for analyzing archaeal GDGTs and long chain alkenones with one instrument exist. For example, Nichols et al. (1993) reported the analysis of *i*GDGTs using high temperature GC and, using an adapted method, Pancost et al. (2008) detected *i*GDGTs and long chain alkenones in the same analytical window. However, such methods are not routinely applied because they are laborious and impacted by various constraints. For example, *i*GDGTs containing OH groups in the biphytane chain are not thermostable if analyzed with GC and the chromatographic resolution is generally worse than for HPLC methods.

Here, we present an extension of the NP-HPLC–APCI-MS method recently described by Becker et al. (2013) to a dedicated protocol for the detection of long chain diols, long chain alkenones and core *i*GDGTs in a single analysis. As proof of concept, we applied the method to sediments deposited since 21 kyr BP in the Sea of Marmara. The interval covers large shifts in climate and environment, like the Last Glacial Maximum (LGM), the Bølling/Allerød (B/A), the Younger Dryas (YD), Sapropel S1 formation and the late Holocene. Furthermore, the Sea of Marmara has oscillated between lacustrine and marine stages following glacial and interglacial global sea level changes, respectively (Stanley and Blanpied, 1980; Ryan et al., 1997, 2003; Aksu et al., 1999, 2002; Çağatay et al., 1999, 2000). The current marine state was established ca. 14.7 kyr BP (e.g. Vidal et al., 2010). This oceanographic history makes the Sea of Marmara an ideal location for studying multiproxy records.

2. Material and methods

2.1. Samples and extraction

Sediment samples were collected during RV Meteor cruise M84/1 ("DARCSEAS I") from different depositional environments (Table 1). Site GeoB15103 is in the Eastern Mediterranean where organic-rich sediments (sapropels) alternate with organic-lean, coccolith-rich sediments. Site GeoB15104 in the Sea of Marmara experiences high terrigenous input and Site GeoB15105 in the Black Sea provides CH_4-rich and organic-rich sediments. After recovery, the samples were immediately frozen and stored at −80 °C until further treatment (Zabel et al., 2011). Additionally, for analysis of alkenones, an *E. huxleyi* culture was used, which had been grown at 23 °C in f/2 medium (Guillard and Ryther, 1962) with a 12 h/12 h light/dark cycle and harvesting at exponential growth phase. For analysis and isolation of long chain diols, surface sediment samples from Aarhus Bay were used (56°07.06′N, 10°20.85′E, 15 m water depth, 10–12 cm and 0–60 cm sediment depth).

Table 1
Sampling site characteristics.

Cruise	Site	Location	Position	Water depth (m)
M84/1	GeoB15103	Eastern Mediterranean	34°01.65′N/ 32°37.80′E	1367
M84/1	GeoB15104	Sea of Marmara	40°47.97′N/ 27°43.49′E	600
M84/1	GeoB15105	Black Sea	41°31.71′N/ 30°53.07′E	1266

The sediment samples (25 ± 0.5 g wet wt), as well as the *E. huxleyi* culture, were extracted using a modified Bligh and Dyer protocol (Sturt et al., 2004): ultrasonication was performed for 10 min in four steps with a mixture of dichloromethane (DCM)/MeOH/buffer (1:2:0.8, v:v:v) using 4 ml solvent/g sediment and extraction step. A phosphate buffer (8.7 g/l KH_2PO_4, pH 7.4) was used for the first two steps, and a CCl_3COOH buffer (50 g/l CCl_3COOH, pH 2) for the final two. After each extraction step, the samples were centrifuged at 800×*g* for 10 min and the supernatants collected in a separation funnel. The combined supernatants were then washed 3× with de-ionized MilliQ water. After separation into organic phase and water-soluble phase, the organic phase was collected as the total lipid extract (TLE). The solvent was gently removed under a stream of N_2 and the extract stored at −20 °C.

2.2. Age model for sediment cores from the Sea of Marmara

The 39 samples from the Sea of Marmara were derived from a 704 cm long gravity core (GeoB15104-1) and a 52 cm multi-core (GeoB15104-2). The sampling interval for the multi-core was 2 cm (26 samples). The gravity core sediments were sampled every ca. 50 cm and covered prominent lithologies, for example the organic rich sediments from the Sapropel S1. The detailed lithology is described by Zabel et al. (2011). The age model for the cores was based on sedimentation rates according to Vidal et al. (2010) for the nearby core MD01-2430. Matching lithologies and interfaces were adjusted, such as the top (7 kyr BP) and bottom (11.5 kyr BP) of S1 and the transition from the marine to the lacustrine sediments (14.7 kyr BP; Fig. S1). Based on this model, the gravity core covered the last ca. 21 kyr.

2.3. Instrumentation

2.3.1. NP-HPLC–APCI-MS

The *i*GDGTs, long chain diols and long chain alkenones were analyzed according to Becker et al. (2013) with a Dionex Ultimate 3000RS UHPLC instrument coupled to a Bruker maXis ultra-high resolution quadrupole time-of-flight mass spectrometer (qToF-MS), equipped with an APCI II ion source. Aliquots of the TLE (typically 10 µl) in *n*-hexane:propan-2-ol (99.5:0.5, v:v) were injected onto two coupled Acquity BEH amide columns (each 2.1 × 150 mm, 1.7 µm; Waters, Eschborn, Germany) kept at 50 °C. Compounds were eluted using the following gradient (after Becker et al., 2013) with eluent A (*n*-hexane) and eluent B [*n*-hexane:propan-2-ol (90:10, v:v)] and constant flow of 0.5 ml/min: 3% B to 5% B in 2 min, to 10% B in 8 min, to 20% B in 10 min, to 50% B in 15 min and to 100% B in 10 min. Columns were washed with 100% B for 6 min and equilibrated with 3% B for 9 min before the next injection.

Compounds were detected in positive ionization mode, scanning from *m/z* 150 to 2000 at 2 scans/s; source parameters were as described by Becker et al. (2013). MS^2 spectra were obtained in data dependent mode. For each MS full scan, up to three MS^2 experiments targeted the most abundant ions with N_2 as collision gas and a collision energy of 35 eV. The isolation width was 6 Da. Active exclusion limited how often a given ion was selected for fragmentation and thus allowed us to obtain MS^2 data for less abundant ions. The mass spectrometer was operated at a resolution of 27,000 at *m/z* 1222 and mass accuracy after calibration by loop injection at the end of each run and by lock mass calibration was typically < 1–2 ppm (cf. Becker et al., 2013). Compounds were assigned from their exact masses and isotope pattern in full scan (MS^1) mode and their characteristic fragmentation in MS^2 spectra. Integration of peaks was performed on extracted ion chromatograms of ± 10 mDa width of the $[M+H]^+$ ion in MS^1 spectra. Accurate mass, high resolution and MS^2 fragment spectra are not essential for quantification of GDGTs, alkenones and diols once the retention time is established; thus, conventional single quadrupole HPLC–MS systems are suitable. Lipid quantification was achieved by injecting an internal standard (C_{46} GTGT; Huguet et al., 2006) along with the samples. The abundances of *i*GDGTs, alkenones and diols were averaged from duplicate measurements; *i*GDGTs and alkenones were corrected for the response factors of GDGT-0 (caldarchaeol), purified from extracts of *Archaeoglobus fulgidus*, and authentic $C_{37:2}$ and $C_{37:3}$ alkenone standards vs. the C_{46} GTGT standard. The lower limit of quantification (LLOQ) for *i*GDGTs and long chain alkenones was < 10 pg. The relative response factor (RRF) between the $C_{37:2}$ and $C_{37:3}$ alkenone was determined to be 1.3, with the higher response for the $C_{37:2}$ alkenone (RF $C_{37:2}$ = 1.3 × RF $C_{37:3}$). For our instrument, the RF values were linear in the range between 10 pg and 10 ng. Since authentic standards for long chain diols were not available, response factor correction and determination of LLOQ was not possible. To determine concentrations of diols we assumed a RRF of 1 vs. the C_{46} GTGT. By assuming this RRF, the LLOQ was < 10 pg.

2.3.2. GC-FID

Alkenoates were removed via base hydrolysis of the TLE fraction following the procedure described by Elvert et al. (2003). GC was performed using a Trace gas chromatograph (ThermoFinnigan GmbH, Bremen, Germany) with a Rxi-5 ms column (30 m × 0.25 mm × 0.25 µm; Restek GmbH, Bad Homburg, Germany) equipped with FID. He served as carrier gas at a constant 1 ml/min. The GC temperature program was: 60 °C (1 min) to 150 °C at 15 °C/min, then to 300 °C (held 28 min) at 4 °C/min. The injector was at 310 °C and the detector at 300 °C. Assignment of di- and triunsaturated C_{37} alkenones ($C_{37:2}$ and $C_{37:3}$) was based on retention times and comparison with parallel GC–MS runs. All samples were analyzed in quadruplicate.

2.3.3. GC–MS

Long chain diols were analyzed using GC–MS with a Trace gas chromatograph system interfaced to a Trace MS instrument (both from ThermoFinnigan) after derivatization with bis(trimethylsilyl) trifluoroacetamide in pyridine at 60 °C for 1 h (Elvert et al., 2003). The mass spectrometer was operated in electron ionization mode (EI^+) at 70 eV over *m/z* 40–700. The ion source was at 200 °C, the interface at 300 °C and He was the carrier gas at a constant 1 ml/min. Samples were injected in splitless mode at 310 °C and separation was achieved with an Rxi-5 ms column (30 m × 0.25 mm × 0.25 µm; Restek GmbH, Bad Homburg, Germany) using the same temperature program as for GC-FID. Assignment of long chain diols was based on retention times and characteristic fragments in the GC–MS run (see Smith et al., 1983; Versteegh et al., 1997). Relevant long chain diols were quantified using extracted ion chromatograms (EICs) of the characteristic fragment ions at *m/z* 299.4, 313.4, 341.4, 327.4, 341.4 and 355.4. All samples were analyzed in duplicate.

2.3.4. Long chain diol isolation

For HPLC-based long chain diol assignment the compounds were isolated from the TLE of the Aarhus Bay sediment sample through reversed phase semi-preparative LC with an Agilent 1200 series HPLC instrument equipped with an Agilent 1200 series fraction collector and coupled to an Agilent 6130 MSD by active splitter. The diols were eluted using the chromatographic protocol of Zhu et al. (2013). In brief, the TLE was fractionated with a semi-preparative Zorbax Eclipse XDB-C_{18} column (5 µm, 250 × 9.4 mm; Agilent Technologies Deutschland GmbH, Böblingen, Germany) operated at 45 °C. Samples were dissolved in MeOH:propan-2-ol (8:2, v:v) and eluted using a linear gradient from 80% MeOH: 20% 2-propanol to 60% MeOH: 40% propan-2-ol in 5 min and then to 35% MeOH: 65% propan-2-ol in another 40 min at 2.2 ml/min. The column was washed with 100% propan-2-ol for 15 min followed by column reconditioning with 100% MeOH for another 15 min. The diols were collected in a time window of 8.6–12 min.

2.3.5. Calculations

TEX_{86} was calculated using the definition of Schouten et al. (2002):

$$TEX_{86} = \frac{[GDGT\text{-}2] + [GDGT\text{-}3] + [GDGT\text{-}5']}{[GDGT\text{-}1] + [GDGT\text{-}2] + [GDGT\text{-}3] + [GDGT\text{-}5']}. \quad (1)$$

where numbers refer to number of rings in the GDGT and GDGT-5′ to the crenarchaeol regio isomer. TEX_{86} was converted to SST using the coretop transfer function of Kim et al. (2008):

$$SST = -10.78 + 56.2\ (TEX_{86}) \quad (2)$$

$U^{K'}_{37}$ was calculated according to Prahl and Wakeham (1987):

$$U^{K'}_{37} = \frac{[C_{37:2}\ \text{alkenone}]}{[C_{37:2}\ \text{alkenone}] + [C_{37:3}\ \text{alkenone}]} \quad (3)$$

It was converted to SST by applying the coretop transfer function of Conte et al. (2006):

$$SST = 29.876(U^{K'}_{37}) - 1.334 \quad (4)$$

LDI was calculated using Eq. 5 as described by Rampen et al. (2012):

$$LDI = \frac{[C_{30}\ 1,15\ \text{diol}]}{[C_{28}\ 1,13\ \text{diol}] + [C_{30}\ 1,13\ \text{diol}] + [C_{30}\ 1,15\ \text{diol}]} \quad (5)$$

SST values were estimated using the global coretop calibration from the same study:

$$SST = \frac{LDI - 0.095}{0.033} \quad (6)$$

Mean deviation for duplicate NP-HPLC–MS runs was ± 0.01 $U^{K'}_{37}$ units (± 0.32 °C), ± 0.006 TEX_{86} units (± 0.31 °C) and ± 0.01 LDI units (± 0.23 °C), respectively, and ± 0.004 $U^{K'}_{37}$ units (0.14 °C) and ± 0.003 TEX_{86} units (0.11 °C), respectively, for HPLC–MS runs. Mean standard deviation for quadruplicate GC-FID runs was ± 0.02 $U^{K'}_{37}$ units (± 0.62 °C) and for duplicate GC–MS runs ± 0.01 LDI units (± 0.28 °C).

The chromatographic resolution (Rs) was calculated from the retention time difference between two adjacent peaks (ΔtR) divided by the sum of their mean peak width at half peak height (W_{avg}):

$$Rs = \frac{\Delta tR}{W_{avg}} \quad (7)$$

3. Results and discussion

The NP-HPLC–APCI-MS method (Becker et al., 2013) allows simultaneous determination of nine paleoenvironmental proxies (Fig. 1a and b): the SST proxies TEX_{86} (Schouten et al., 2002), $U^{K'}_{37}$ (Brassell et al., 1986) and LDI (Rampen et al., 2012), the proxy for terrigenous input to the ocean using the branched isoprenoid tetraether index (BIT; Hopmans et al., 2004), proxies for annual mean air temperature (MAT) and soil pH using the cyclisation (CBT) and methylation ratio of branched tetraethers (MBT; Weijers et al., 2007), a proxy for paleosalinity using the archaeol and caldarchaeol ecometric (ACE; Turich and Freeman, 2011), a proxy for past methane hydrate dissociation using the methane index (MI; Zhang et al., 2011) and a SST proxy for high latitudes via hydroxylated *i*GDGT-based indices (Huguet et al., 2013). Additionally, the whole suite of recently identified tetraether core lipids from Liu et al. (2012) and Zhu et al. (2014), such as *br*GDGTs with a higher and lower degree of methylation than the regular compounds, and butane- and pentanetriol dialkyl glycerol tetraethers, could be detected (Fig. 1b). Their ecological and environmental significance needs, however, to be clarified. We demonstrate below the extension of the HPLC–MS protocol of Becker et al. (2013) to the analysis of $U^{K'}_{37}$ and LDI, i.e. to the simultaneous analysis of three molecularly independent SST proxies in a single analysis (see Fig. 1), which is not possible with the conventional protocols due to inadequate chromatographic separation of the proxy-relevant alkenones and diols, respectively.

3.1. Detection of long chain alkenones using HPLC–MS

In the NP-HPLC base peak chromatogram (BPC) of the TLE of the *E. huxleyi* culture (Fig. 2a) the long chain alkenones eluted between 1.8 and 2.5 min. They were unambiguously assigned from their exact mass in full scan (MS^1) spectra and their characteristic fragmentation in MS^2 spectra. The major product ion of the $C_{37:2}$ alkenone ($[M+H]^+$ at *m/z* 531.5499) is *m/z* 513.5394 (−18.0 Da), formed by loss of water (Fig. 2b). The remaining larger fragments form a series with 14.0 Da difference between the product ions, resulting from cleavage between different carbons after initial loss of water. For example, the fragment at *m/z* 317.3203 results from cleavage between C-23 and C-24 and that at *m/z* 331.3359 from cleavage between C-24 and C-25. The C=C locations cannot be determined using MS without derivatization, because they can migrate when the alkyl chain is ionized (López and Grimalt, 2004; Rontani et al., 2006). The C_{38} and C_{39} Et ketones elute before the C_{37} and C_{38} Me ketones and the $C_{37:2}$ and $C_{37:3}$ alkenones are well separated (see Fig. 2a) and can be quantified readily for computation of $U^{K'}_{37}$. The chromatographic resolution according to Eq. 7 between the two peaks is 1.12. Resolving them is necessary, since otherwise the $^{13}C_2$ isotope peak from $C_{37:3}$ would contribute to the monoisotopic peak of the $C_{37:2}$ alkenone. The co-elution of the C_{38} and C_{37} Me ketones does not influence their quantification because of the MS-based detection and a difference of 14.0 Da between the C_{37} and C_{38} alkenones. The $C_{37:4}$ alkenone was not detected in the *E. huxleyi* culture, presumably because of the relatively high culture temperature (23 °C), at which only small amounts of the $C_{37:4}$ alkenones are produced (Prahl et al., 1988).

Having demonstrated the detection of alkenones with NP-HPLC–MS, we were able to measure TEX_{86} and $U^{K'}_{37}$ in a single analysis (e.g. Fig. 2c). This brings the advantages of eliminating sample preparation steps, e.g. base hydrolysis to remove alkenoates, highly reduced time for analysis, and increased sensitivity of one order of magnitude compared with conventional GC based methods. The limit of quantification for the new method is < 10 pg, whereas for GC-FID it is generally in the ng range (e.g. Villanueva and Grimalt, 1997). Potential disadvantages of analyzing alkenones with HPLC–MS could be changes in the relative sensitivity between the di- and triunsaturated compounds and non-linear response factors, as observed with other MS methods, e.g. GC-CI-MS (Chaler et al., 2000, 2003), GC-EI-MS (Versteegh et al., 2001) and GC-qToF-MS (Hefter, 2008). In order to quantify such effects, we calibrated our

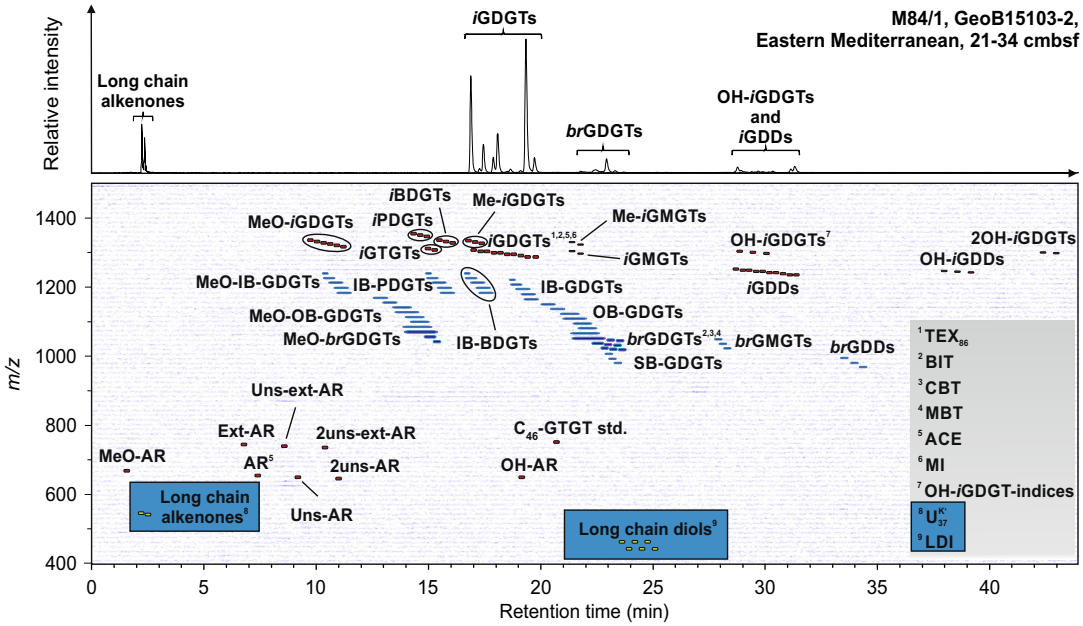

Fig. 1. (a) Reconstructed NP-UHPLC–APCI-qToF-MS base peak chromatogram showing long chain alkenones, *i*GDGTs, brGDGTs, *i*GDDs and OH-*i*GDGTs in sample M84/1, GeoB15103-2, 21–34 cmbsf. (b) Associated reconstructed density map plot showing whole range of lipid biomarkers detectable with the NP-HPLC–APCI-MS protocol, as well as long chain alkenones and diols (blue boxes). Superscripts indicate proxies that can be determined from specific lipids or lipid groups. Abbreviations (according to Liu et al., 2012 and Zhu et al., 2014): GDGT, glycerol dialkyl glycerol tetraether; GDD, glycerol dialkanol diether; GMGT, glycerol monoalkyl glycerol tetraether; BDGT, butanetriol dialkyl glycerol tetraether; PDGT, pentanetriol dialkyl glycerol tetraether; GTGT, glycerol trialkyl glycerol tetraether; AR, archaeol; OH, monohydroxy; 2OH, dihydroxy; Uns, monounsaturated; 2uns, diunsaturated; Ext, extended; Me, methylated; MeO, methoxy; *i*, isoprenoid; *br*, branched; IB, hybrid isoprenoid/branched; OB, overly branched; SB, sparsely branched (for interpretation of the references to color in this figure legend, the reader is referred to the web version of the article).

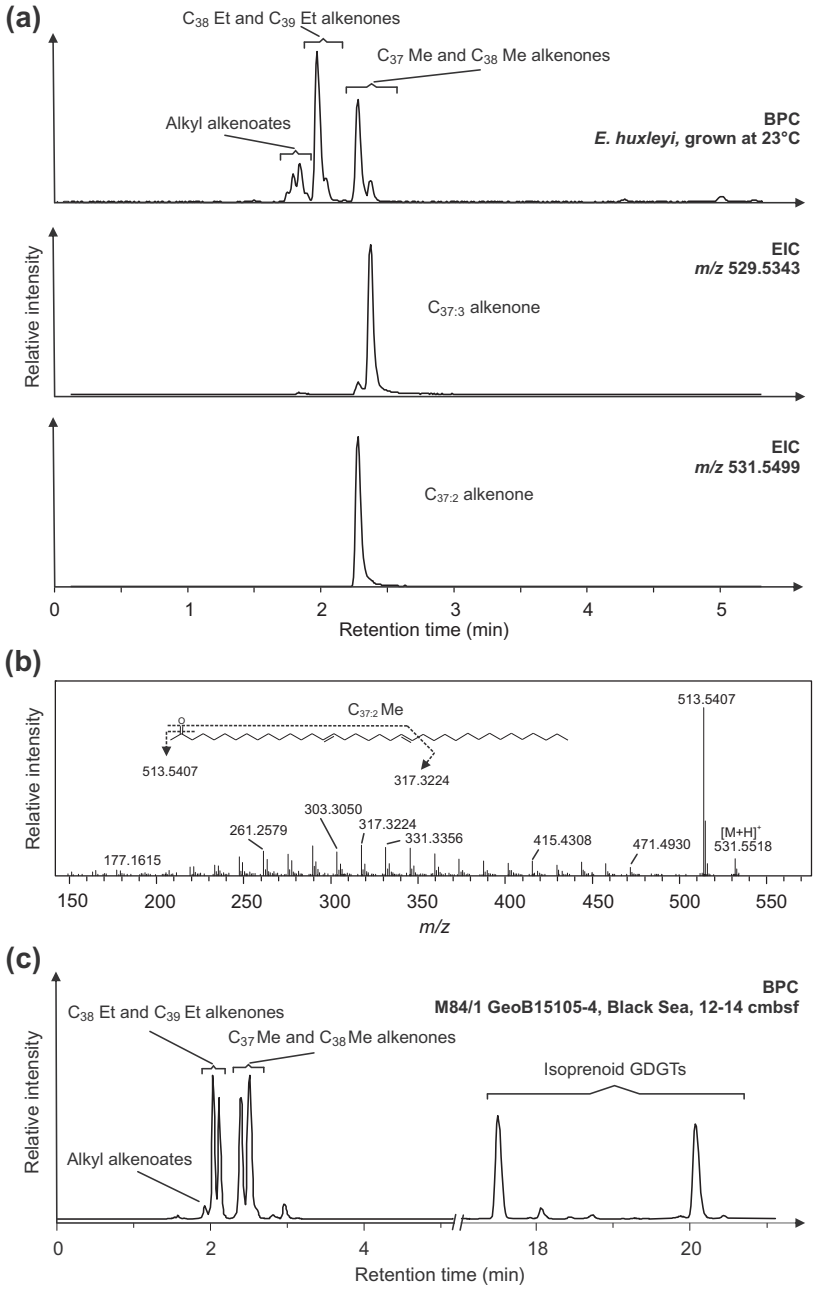

Fig. 2. (a) NP-HPLC–APCI-MS base peak chromatogram (BPC) showing long chain alkenones and alkyl alkenoates, and extracted ion chromatograms (EICs) showing the triunsaturated (*m/z* 529.5) and diunsaturated (*m/z* 531.5) alkenones in the TLE of *E. huxleyi*. (b) NP-HPLC–APCI-multiple stage mass spectrum (MS^2) of the diunsaturated alkenone ($[M+H]^+$at *m/z* 531.5). Shown are the MS^2 fragment ions within the range *m/z* 150–570. The structure and formation of the major product ions are also indicated. (c) NP-HPLC–APCI-MS BPC showing long chain alkenones and *i*GDGTs in the TLE from the marine sediment M84/1 GeoB15105-4, Black Sea, 12–14 cmbsf.

instruments with the $C_{37:2}$ and $C_{37:3}$ alkenone standards. The RRF values slightly differed between the two compounds but were linear for our instrument. Thus, the monitoring of RRF is recommended for the use of the presented protocol, which applies for MS-based detection in general.

3.2. Detection of long chain diols using HPLC–MS

Detection of long chain alkenones with NP-HPLC–MS led us to further inspect the protocol for the detection of long chain diols, which are used for the LDI SST proxy. Their greater polarity than the long chain alkenones results in a longer retention time in the NP-HPLC chromatogram. Indeed, in the BPC of the isolated long chain diol fraction from the Aarhus Bay sediment, the diols eluted between 24 and 27 min (Fig. 3). They were tentatively assigned from the exact mass in full scan (MS^1), the characteristic fragmentation in MS^2 spectra and by comparison of the relative distribution of the major diol isomers with that obtained through conventional GC–MS.

The diols are subject to in-source dehydration during the protocol for NP-HPLC–APCI-MS, with the resulting dehydrated fragment (−18.0 Da). For example, the major MS^1 signal for the C_{30} diols was at *m/z* 437.4171 and for the C_{28} diols at *m/z* 409.4404. For accurate quantification, we therefore propose to use the dehydrated fragments.

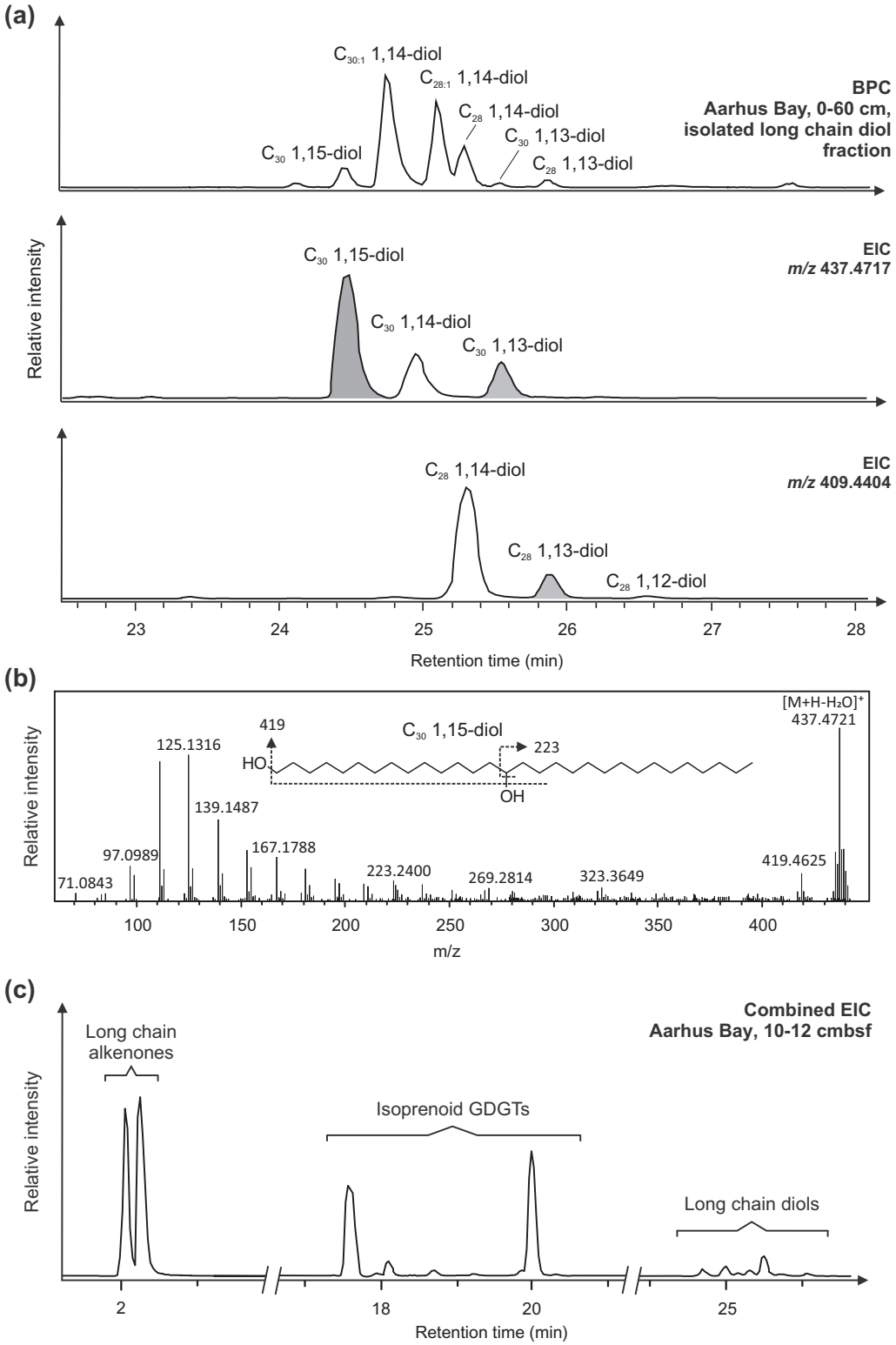

Fig. 3. (a) NP-HPLC–APCI-MS BPC showing long chain diols, and EICs showing the C_{30} (*m/z* 437.4) and the C_{28} (*m/z* 409.4) diols in the isolated long chain diol fraction from the Aarhus Bay sediment sample, 0–60 cmbsf. Gray shaded peaks indicate the diols used for the LDI SST proxy. (b) NP-HPLC–APCI-multiple stage mass spectrum (MS^2) of the C_{30} 1:15 diol ($[M+H]^+ - 18$ Da at *m/z* 437.4). Shown are the MS^2 fragment ions within the range *m/z* 60–450. The structure and the formation of the major product ions are also shown. (c) NP-HPLC–APCI-MS BPC showing long chain alkenones, long chain diols and *i*GDGTs in the TLE of the marine sediment from Aarhus Bay, 10–12 cmbsf.

In the MS^2 spectrum of the C_{30} 1:15 diol ($[M+H]^+$ −18.0 Da at *m/z* 437.4171) the major fragment was at *m/z* 419.4611 (Fig. 3b), representing loss of the second OH group (−18.0 Da). The remaining larger fragments form a series with 14.0 Da difference between the product ions resulting from cleavage between different carbons after loss of the OH groups. Like the fragmentation of the long chain alkenones, C=C positions in the diol derivatives, obtained via loss of the OH groups, cannot be determined with MS^2. Therefore, the identity of the isomers with the same chain length cannot be determined using this method. However, comparison

of the relative abundance of the major diol isomers between the conventional GC–MS method and the NP-HPLC protocol (Table 2) indicates that retention is based on compound polarity, so the earliest eluting major peak was the C_{30} 1,15 diol, the second with the same mass the C_{30} 1,14 diol and the third the C_{30} 1,13 diol, i.e. in order of increasing polarity. The major C_{28} diols were (early to late eluting): C_{28} 1,14, C_{28} 1,13 and C_{28} 1,12. The isomers used for LDI were baseline separated (see Fig. 3a) and could be quantified readily for determination of LDI. The NP-HPLC protocol therefore enables the determination of the three proxies – TEX_{86}, $U^{K'}_{37}$ and LDI from a single analysis (Fig. 3c, Fig. 4a).

The simultaneous detection of the three SST proxies might also be possible with conventional single quadrupole HPLC–MS systems, since the pressure using the presented method is below the upper limit for most HPLC instruments (600 bar), but would require method development including the adjustment of ionization parameters as well as of the gradient system for the columns used here. As an alternative to the two coupled amide columns, the use of a single column results in adequate separation of alkenones and diols (data not shown) and the maximum pressure is < 400 bar. However, *i*GDGT and *i*GDD isomers cannot be fully resolved under these conditions (Becker et al., 2013). The establishment of the retention times of long chain diols and alkenones should be based on standard compounds or isolated fractions as described here (i.e. alkenones from an *E. huxleyi* culture or long chain diols from marine sediments). The high sensitivity of the qToF-MS enables detection of the relevant compounds in full scan mode, which is likely not possible with a single quadrupole MS instrument. As for GDGTs, detection should be performed in selective ion monitoring (SIM) mode, scanning only for the masses of alkenones (as $[M+H]^+$ ions; see Fig. 2) and diols (as $[M+H-H_2O]^+$; see Fig. 3).

3.3. Comparison of $U^{K'}_{37}$ determined with GC-FID and HPLC–MS

The GC-FID based $U^{K'}_{37}$ values for samples from the Eastern Mediterranean, the Black Sea and selected samples from the Sea of Marmara core varied between 0.21 ± 0.05 and 0.82 ± 0.05 (providing SST between 5.4 ± 1.7 and 23.4 ± 1.5 °C) and thus cover a wide range of the possible $U^{K'}_{37}$ scale (Fig. 4a and b; Table 3). The relatively large error for quadruplicate GC-FID runs (precision of 0.02 $U^{K'}_{37}$ units) might result from the low amounts of the $C_{37:2}$ and $C_{37:3}$ alkenones injected on-column especially for the sediment samples (Grimalt et al., 2001). In contrast, standard deviation for quadruplicate runs of the *E. huxleyi* culture, which contained alkenones at considerably higher abundance, was 0.004 and thus within the range generally obtained (Herbert, 2003). The maximum discrepancy between NP-HPLC and GC for $U^{K'}_{37}$ was 0.12 ± 0.03 (sample GeoB15103-2, 21–43 cm below sea floor, cmbsf), representing a temperature difference of 3.5 ± 0.8 °C. For most samples, the discrepancy was within the standard error for most calibrations (± 0.7–1.6 °C). The mean $\Delta_{UK'37}$ between GC and NP-HPLC analysis was ± 0.05. The linear relationship between NP-HPLC and GC $U^{K'}_{37}$ (r^2 0.93, slope 0.95; Fig. 4b) shows that the protocol provides reliable and reproducible results for $U^{K'}_{37}$.

3.4. Comparison of LDI determined with GC–MS and HPLC–MS

LDI values determined from GC–MS in the sample set as above varied between 0.58 ± 0.01 and 0.98 ± 0.0007, providing SST values between 14.7 ± 0.2 and 26.8 ± 0.06 °C (Table 3, Fig. 4a). LDI values from NP-HPLC and GC–MS show a clear linear relationship (r^2 0.95, slope 0.88; Fig. 4c), demonstrating that the NP-HPLC protocol provides robust results for LDI. For most samples, the discrepancy between NP-HPLC and GC LDI was within the standard error for the most recent calibration (± 2 °C, Rampen et al., 2012). The mean Δ_{LDI} for the samples was ± 0.03 and the mean Δ_T ± 0.88 °C. The maximum discrepancy between NP-HPLC and GC LDI was

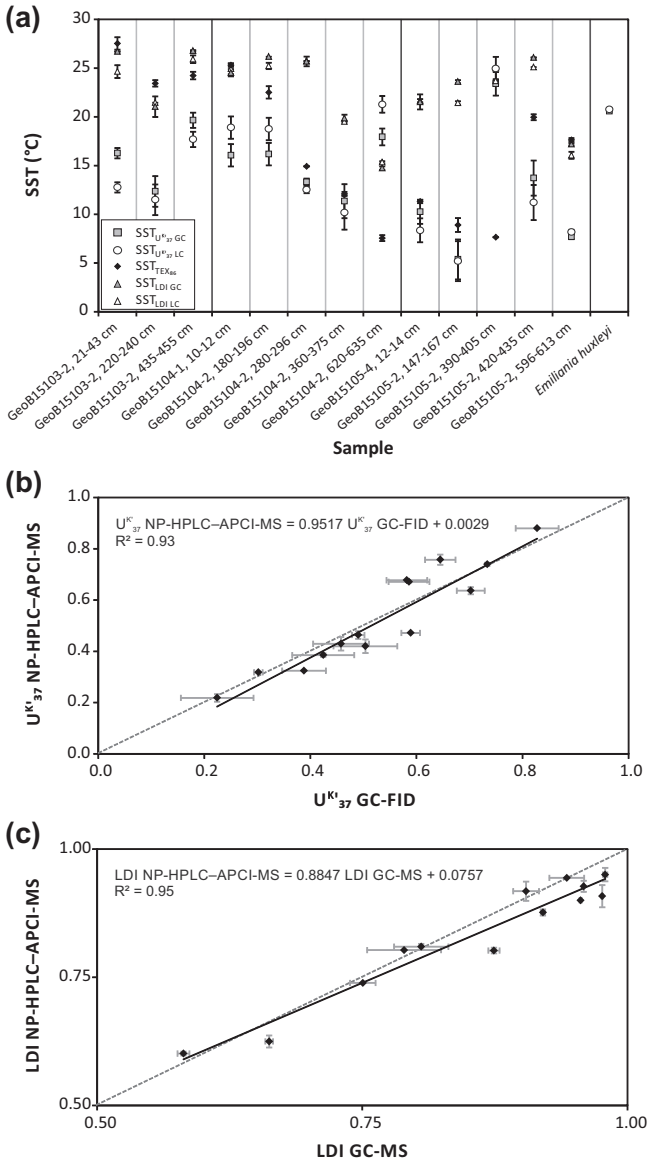

Fig. 4. (a) SST values for different marine sediments and *E. huxleyi* culture. Shown are the alkenone-based temperatures determined from GC-FID ($SST_{UK'37\ GC}$) and NP-HPLC–APCI-MS ($SST_{UK'37\ LC}$), the diol-based temperatures determined from GC–MS ($SST_{LDI\ GC}$) and NP-HPLC–APCI-MS ($SST_{LDI\ LC}$) and archaeal GDGT-derived temperature (SST_{TEX86}) determined from NP-HPLC–APCI-MS. Error bars indicate deviation for replicate analysis. (b) Cross plot of $U^{K'}_{37}$ values determined using GC-FID and NP-HPLC–APCI-MS. (c) Cross plot of LDI values determined using GC–MS and NP-HPLC–APCI-MS. Dashed lines in each cross plot indicates the 1:1 line.

Table 2
Fractional abundance (%) of major long chain diols and LDI in isolated diol fraction from Aarhus Bay sediment determined with GC–MS and NP-HPLC–MS, respectively.

	C_{28} 1,12 diol	C_{28} 1,13 diol	C_{28} 1,14 diol	C_{30} 1,13 diol	C_{30} 1,14 diol	C_{30} 1,15 diol	LDI
GC–MS (n = 3)	1.55 ± 0.46	10.21 ± 0.04	50.72 ± 9.93	4.88 ± 1.76	8.12 ± 2.67	24.53 ± 5.99	0.62 ± 0.03
NP-HPLC–MS (n = 3)	1.35 ± 0.32	9.78 ± 0.79	50.03 ± 0.77	5.46 ± 0.57	10.16 ± 1.89	23.23 ± 3.20	0.60 ± 0.04

Table 3
$U^{K'}_{37}$, LDI, TEX_{86} and corresponding SST values with different methods.

		GC-FID		GC-MS		NP-HPLC-APCI-MS					
Core (GeoB)	Depth interval (cmbsf)	$U^{K'}_{37}$	SST	LDI	SST	$U^{K'}_{37}$	SST	TEX_{86}	SST	LDI	SST
15103-2	21–34	0.59 ± 0.02	16.27 ± 0.58	0.98 ± 0.0007	26.70 ± 0.02	0.47 ± 0.001	12.76 ± 0.03	0.68 ± 0.01	27.53 ± 0.63	0.91 ± 0.02	24.64 ± 0.65
15103-2	220–240	0.46 ± 0.05	12.35 ± 1.57	0.79 ± 0.03	21.04 ± 1.05	0.43 ± 0.03	11.49 ± 0.79	0.61 ± 0.01	23.44 ± 0.33	0.80 ± 0.001	21.45 ± 0.001
15103-2	435–455	0.70 ± 0.03	19.65 ± 0.91	0.98 ± 0.002	26.79 ± 0.06	0.64 ± 0.02	17.69 ± 0.51	0.62 ± 0.01	24.24 ± 0.39	0.95 ± 0.01	25.92 ± 0.40
15104-1	42348	0.58 ± 0.04	16.05 ± 1.25	0.90 ± 0.01	24.53 ± 0.37	0.68 ± 0.03	18.9 ± 0.84	0.64 ± 0.003	25.3 ± 0.17	0.92 ± 0.02	24.93 ± 0.56
15104-2	180–196	0.59 ± 0.04	16.17 ± 1.25	0.96 ± 0.0001	26.17 ± 0.00	0.67 ± 0.003	18.79 ± 0.10	0.59 ± 0.01	22.51 ± 0.63	0.93 ± 0.01	25.23 ± 0.33
15104-2	280–296	0.49 ± 0.02	13.3 ± 0.35	0.94 ± 0.02	25.69 ± 0.50	0.46 ± 0.01	12.51 ± 0.19	0.46 ± 0.0002	14.93 ± 0.01	0.94 ± 0.001	25.72 ± 0.003
15104-2	360–375	0.42 ± 0.06	11.34 ± 1.70	0.75 ± 0.01	19.86 ± 0.36	0.39±0.03	10.18 ± 0.76	0.41 ± 0.003	12.10 ± 0.21	0.74 ± 0.001	19.51 ± 0.01
15104-2	620–635	0.65 ± 0.05	17.94 ± 0.97	0.58 ± 0.01	14.74 ± 0.17	0.76 ± 0.0001	21.29 ± 0.01	0.33 ± 0.01	7.56 ± 0.30	0.61 ± 0.004	15.34 ± 0.08
15105-4	12–14	0.39 ± 0.04	10.26 ± 1.19	0.81 ± 0.03	21.53 ± 0.78	0.32 ± 0.001	8.36 ± 0.02	0.39 ± 0.003	11.31 ± 0.18	0.81 ± 0.01	21.66 ± 0.16
15105-2	147–167	0.22 ± 0.06	5.37 ± 1.71	0.87 ± 0.01	23.61 ± 0.16	0.22 ± 0.01	5.19 ± 0.34	0.35 ± 0.01	8.90 ± 0.71	0.80 ± 0.01	21.43 ± 0.17
15105-2	390–405	0.83 ± 0.05	23.39 ± 1.52	0.92 ± 0.001	25.01 ± 0.06	0.88 ± 0.002	24.95 ± 0.07	0.33 ± 0.0002	7.65 ± 0.01	0.88 ± 0.01	23.68 ± 0.18
15105-2	420–435	0.50 ± 0.06	13.72 ± 1.85	0.96 ± 0.001	26.08 ± 0.03	0.42 ± 0.03	11.21 ± 0.78	0.55 ± 0.01	19.96 ± 0.30	0.90 ± 0.001	25.10 ± 0.001
15105-2	596–613	0.30 ± 0.01	7.69 ± 0.22	0.66 ± 0.003	17.19 ± 0.11	0.32 ± 0.001	8.17 ± 0.02	0.51 ± 0.003	17.64 ± 0.18	0.60 ± 0.02	16.05 ± 0.66
Emiliania huxleyi		0.73 ± 0.01	20.58 ± 0.15	–	–	0.74 ± 0.01	20.75 ± 0.26	–	–	–	–

0.07 ± 0.01 for GeoB15105-2, 147–167 cmbsf, representing a difference of 2.2 ± 0.3 °C.

3.5. SST estimates from different proxies

The substantially higher TEX_{86} than $U^{K'}_{37}$ SST estimates for most samples obtained from the NP-HPLC analysis (Fig. 4a, Table 3) might be explained by differences in ecology of the relevant haptophyta and archaea, such as production season or water depth. A similar pattern has been observed for the Mediterranean Gulf of Taranto, where the $U^{K'}_{37}$ signal corresponds to winter SST and the offshore TEX_{86} signal to summer SST (Leider et al., 2010). Only two samples showed the opposite behavior, i.e. higher $U^{K'}_{37}$ than TEX_{86} SST estimates. One originates from the Black Sea sapropel, an interval of strong (upper) water column stratification, and the anomalous signal at this site could be explained by a strong contribution of deeper dwelling planktonic archaea that thrive in the colder chemocline, an explanation also suggested by Menzel et al. (2006). However, this is in contrast to studies of modern subsurface GDGT distributions, which showed a warm bias for the TEX_{86} signal (Schouten et al., 2012; Basse et al., 2014; Hernández-Sánchez et al., 2014; Xie et al., 2014). The LDI-derived temperature values are generally higher than those from $U^{K'}_{37}$ and TEX_{86} for corresponding samples (Fig. 4a), except for the Eastern Mediterranean, where TEX_{86}-derived temperatures are equal to or slightly higher than those derived from the LDI. This warm bias of LDI-derived temperatures was also observed by Lopes dos Santos et al. (2013). The authors compared LDI-inferred and foraminiferal assemblage-derived temperature values for the Southern Ocean and suggested that the LDI reflects SST of the warmest month. The ecological factors that might influence the lipid distribution of the signal producers and therefore the proxies are discussed in the next section. Lateral sediment transport and selective aerobic degradation during early diagenesis may also contribute to differences between SST from alkenones and *i*GDGTs (e.g. Huguet et al., 2009; Kim et al., 2009).

3.6. Past SST variation in the Sea of Marmara determined with the new protocol

Alkenones, diols and *i*GDGTs were detected in all samples in sufficiently adequate concentration for proxy estimations (Fig. 5a and b; Table S1). Total *i*GDGT concentration varied between 0.44 and 8.58 μg/g sediment dry wt (sed. dw) all along the record. The maximum concentration occurred within S1. A second peak was observed in the sample from the B/A with a

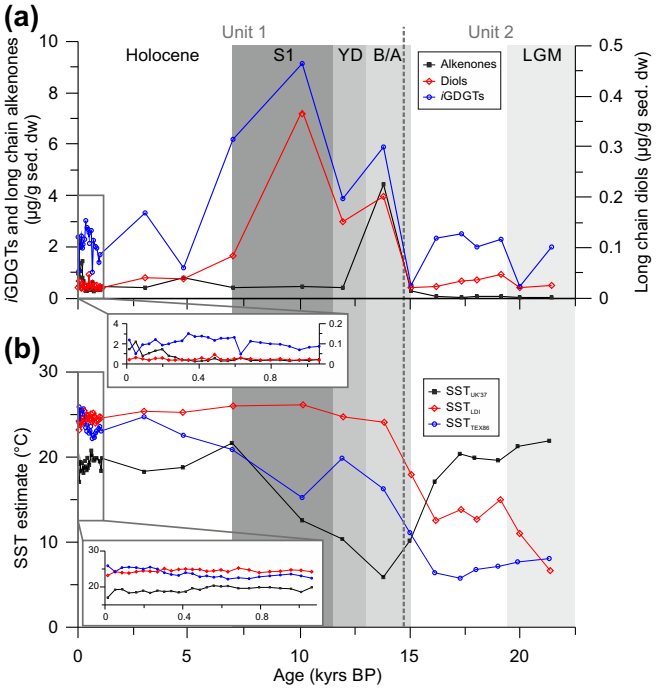

Fig. 5. (a) Total *i*GDGT, diol and alkenone concentrations (μg/g sed. dw) vs. age. The timing of the major climatic events is also denoted. (b) SST estimates for cores GeoB15104-2 and -4 from the Sea of Marmara based on alkenones ($SST_{UK'37}$), diols (SST_{LDI}) and archaeal *i*GDGTs (SST_{TEX86}) determined from NP-HPLC–APCI-MS. The timing of the Younger Dryas (YD), Bølling/Allerød (B/A), Sapropel S1 (S1), Last Glacial Maximum (LGM), Holocene and marine (Unit 1) and lacustrine (Unit 2) units are denoted.

concentration of 5.81 μg/g sed. dw. Total diol concentration followed a similar pattern but absolute values were one to two orders of magnitude lower than for *i*GDGTs. In contrast, total alkenone concentration showed no distinct peak in S1. The maximum concentration occurred in the sample from the B/A at 4.45 μg/g sed. dw. Lowest concentration was in samples from the lacustrine stage (0.02–0.07 μg/g sed. dw). For these samples, alkenones characteristic of freshwater environments (Thiel et al., 1997; Schulz et al., 2000) were not detected. For the Holocene samples, alkenone concentration ranged between 2.22and 0.80 μg/g sed. dw in the top 15 cm of the record, whereas it was ca. 0.41 μg/g sed. dw for the deeper samples (Table 1). The alkenone and diol concentration profiles are in line with previous studies (Vidal et al., 2010) and

Table 4
$U^{K'}_{37}$, LDI, TEX_{86} and corresponding SST values for sediment cores from the Sea of Marmara.

Core	Coring device	Depth interval (cmbsf)	Estimated age (kyr BP)	$U^{K'}_{37}$	TEX_{86}	LDI	$SST_{UK'37}$ (°C)	SST_{TEX86} (°C)	SST_{LDI} (°C)
GeoB15104-1	MUC	0–2	0.01	0.62 ± 0.02	0.65 ± 0.02	0.86 ± 0.05	17.09 ± 0.59	25.95 ± 0.86	23.2 ± 1.42
GeoB15104-1	MUC	2–4	0.05	0.69 ± 0.001	0.62 ± 004	0.89 ± 0.02	19.24 ± 0.01	24.25 ± 0.20	24.22 ± 0.49
GeoB15104-1	MUC	4–6	0.09	0.69 ± 0.03	0.64 ± 0.01	0.88 ± 0.02	19.35 ± 0.87	25.33 ± 0.47	23.91 ± 0.47
GeoB15104-1	MUC	6–8	0.12	0.66 ± 0.06	0.65 ± 0.01	0.88 ± 0.04	18.34 ± 1.82	25.49 ± 0.69	23.84 ± 1.06
GeoB15104-1	MUC	8–10	0.16	0.66 ± 0.01	0.64 ± 0.01	0.89 ± 0.05	18.39 ± 0.16	25.37 ± 0.41	24.18 ± 1.45
GeoB15104-1	MUC	10–12	0.20	0.68 ± 0.03	0.64 ± 0.003	0.92 ± 0.02	18.9 ± 0.84	25.3 ± 0.17	24.93 ± 0.56
GeoB15104-1	MUC	12–14	0.23	0.66 ± 0.03	0.65 ± 0.02	0.90 ± 0.02	18.26 ± 0.84	25.51 ± 1.29	24.39 ± 0.72
GeoB15104-1	MUC	14–16	0.27	0.68 ± 0.01	0.64 ± 0.003	0.89 ± 0.01	19.02 ± 0.31	25.02 ± 0.15	24.17 ± 0.23
GeoB15104-1	MUC	16–18	0.31	0.67 ± 0.02	0.62 ± 0.01	0.93 ± 0.02	18.75 ± 0.51	23.94 ± 0.33	25.15 ± 0.54
GeoB15104-1	MUC	18–20	0.34	0.67 ± 0.03	0.61 ± 0.01	0.90 ± 0.01	18.77 ± 0.95	23.51 ± 0.76	24.53 ± 0.16
GeoB15104-1	MUC	20–22	0.38	0.66 ± 0.02	0.61 ± 0.01	0.91 ± 0.01	18.47 ± 0.71	23.22 ± 0.44	24.84 ± 0.15
GeoB15104-1	MUC	22–24	0.41	0.67 ± 0.01	0.62 ± 0.01	0.92 ± 0.01	18.71 ± 0.28	23.96 ± 0.29	24.97 ± 0.16
GeoB15104-1	MUC	24–26	0.45	0.70 ± 0.01	0.61 ± 0.01	0.92 ± 0.01	19.66 ± 0.41	23.69 ± 0.42	24.91 ± 0.26
GeoB15104-1	MUC	26–28	0.49	0.69 ± 0.01	0.60 ± 0.01	0.92 ± 0.02	19.2 7 ± 0.16	22.77 ± 0.74	24.88 ± 0.56
GeoB15104-1	MUC	28–30	0.52	0.71 ± 0.01	0.60 ± 0.01	0.90 ± 0.01	19.88 ± 0.38	23.02 ± 0.51	24.34 ± 0.44
GeoB15104-1	MUC	30–32	0.56	0.73 ± 0.05	0.60 ± 0.01	0.90 ± 0.01	20.41 ± 1.57	22.64 ± 0.63	24.54 ± 0.19
GeoB15104-1	MUC	32–34	0.60	0.72 ± 0.01	0.60 ± 0.003	0.91 ± 0.01	20.14 ± 0.38	22.99 ± 0.19	24.74 ± 0.42
GeoB15104-1	MUC	34–36	0.63	0.72 ± 0.03	0.59 ± 0.01	0.89 ± 0.001	20.30 ± 0.83	22.15 ± 0.77	24.20 ± 0.12
GeoB15104-1	MUC	36–38	0.69	0.70 ± 0.01	0.59 ± 0.005	0.93 ± 0.02	19.58 ± 0.27	22.51 ± 0.28	25.20 ± 0.61
GeoB15104-1	MUC	38–40	0.74	0.70 ± 0.02	0.59 ± 0.01	0.91 ± 0.01	19.60 ± 0.51	22.32 ± 0.82	24.67 ± 0.36
GeoB15104-1	MUC	40–42	0.79	0.71 ± 0.02	0.60 ± 0.01	0.89 ± 0.01	19.90 ± 0.67	22.86 ± 0.32	24.02 ± 0.34
GeoB15104-1	MUC	42–44	0.85	0.71 ± 0.01	0.60 ± 0.01	0.90 ± 0.01	19.89 ± 0.25	23.12 ± 0.49	24.25 ± 0.19
GeoB15104-1	MUC	44–46	0.90	0.7 ± 0.003	0.61 ± 0.03	0.90 ± 0.02	19.55 ± 0.08	23.35 ± 1.43	24.40 ± 0.67
GeoB15104-1	MUC	46–48	0.96	0.7 ± 0.02	0.61 ± 0.002	0.91 ± 0.03	19.49 ± 0.69	23.54 ± 0.11	24.75 ± 0.81
GeoB15104-1	MUC	48–50	1.01	0.67 ± 0.07	0.6 ± 0.009	0.91 ± 0.03	18.56 ± 1.98	23.08 ± 0.49	24.65 ± 0.76
GeoB15104-1	MUC	50–52	1.06	0.71 ± 0.01	0.59 ± 0.02	0.89 ± 0.003	19.82 ± 0.17	22.48 ± 0.95	24.16 ± 0.09
GeoB15104-2	GRC	116–130	3.01	0.66 ± 0.01	0.63 ± 0.01	0.93 ± 0.01	18.29 ± 0.33	24.73 ± 0.59	25.35 ± 0.44
GeoB15104-2	GRC	180–196	4.76	0.67 ± 0.003	0.59 ± 0.01	0.93 ± 0.01	18.79 ± 0.10	22.51 ± 0.63	25.23 ± 0.33
GeoB15104-2	GRC	222–236	6.95	0.77 ± 0.02	0.56 ± 0.01	0.95 ± 0.01	21.70 ± 0.67	20.94 ± 0.39	25.97 ± 0.34
GeoB15104-2	GRC	280–296	10.10	0.46 ± 0.01	0.46 ± 0.0002	0.94 ± 0.001	12.51 ± 0.19	14.93 ± 0.01	25.72 ± 0.003
GeoB15104-2	GRC	310–325	11.91	0.39 ± 0.02	0.55 ± 0.02	0.91 ± 0.01	10.34 ± 0.63	19.88 ± 1.12	24.76 ± 0.37
GeoB15104-2	GRC	340–355	13.76	0.24 ± 0.01	0.48 ± 0.01	0.89 ± 0.03	5.86 ± 0.22	16.3 ± 0.401	24.12 ± 0.85
GeoB15104-2	GRC	360–375	14.99	0.39 ± 0.03	0.41 ± 0.003	0.74 ± 0.001	10.18 ± 0.76	12.10 ± 0.21	19.51 ± 0.01
GeoB15104-2	GRC	420–435	16.12	0.62 ± 0.03	0.31 ± 0.01	0.51 ± 0.05	17.12 ± 0.88	6.38 ± 0.78	12.57 ± 1.47
GeoB15104-2	GRC	480–495	17.24	0.73 ± 0.03	0.29 ± 0.02	0.55 ± 0.04	20.41 ± 0.97	5.69 ± 0.94	13.80 ± 1.31
GeoB15104-2	GRC	517–532	17.94	0.71 ± 0.04	0.31 ± 0.02	0.51 ± 0.05	19.89 ± 1.33	6.71 ± 1.01	12.59 ± 1.503
GeoB15104-2	GRC	575–588	19.01	0.70 ± 0.02	0.32 ± 0.01	0.59 ± 0.01	19.54 ± 0.52	7.13 ± 0.64	14.95 ± 0.29
GeoB15104-2	GRC	620–635	19.87	0.76 ± 0.001	0.33 ± 0.01	0.61 ± 0.012	21.29 ± 0.01	7.56 ± 0.30	15.34 ± 0.08
GeoB15104-2	GRC	690–704	21.29	0.78 ± 0.03	0.33 ± 0.01	0.31 ± 0.02	21.94 ± 0.96	8.02 ± 0.29	6.58 ± 0.63

suggest that haptophytes were important in the phytoplanktonic community before the sapropel formation right after the marine connection of the Sea of Marmara. The high concentration of total *i*GDGTs and diols in S1 can be attributed to both increased primary production and preservation of organic matter (e.g. Sperling et al., 2003).

$U^{K'}_{37}$, TEX_{86} and LDI-derived temperature estimates are similar for the late Holocene (7 to 0 kyr BP) with high and largely invariable values, although absolute values for the $U^{K'}_{37}$ derived SSTs are consistently lower than those derived from TEX_{86} and LDI (Fig. 5b). Reconstructed temperature values from $U^{K'}_{37}$ ($SST_{UK'37}$) are 17.0 to 20.5 °C, from TEX_{86} (SST_{TEX86}) 22.2 to 26.0 °C and from LDI (SST_{LDI}) 23.2 to 25.4 °C (Table 4). Between the LGM and S1, the temperature records differ. In the LGM, the $SST_{UK'37}$ shows its highest temperature (21.9 °C), which decreases during the transition from the LGM to the B/A, reaching 5.9 °C in the B/A. From the B/A to S1, $SST_{UK'37}$ increases again, reaching 21.7 °C at the top of S1. In contrast to $SST_{UK'37}$, SST_{LDI} and SST_{TEX} are relatively low for the last glacial, with constant SST_{TEX86} of ca. 7 °C and T_{LDI} between 6.6 (at 21.3 kyr) and 15.3 °C. SST_{TEX86} and SST_{LDI} increase during the transition from the glacial to the B/A. SST_{LDI} reaches modern Holocene values during the B/A. However, the warming trend for SST_{TEX86} starting at ca. 15.2 kyr is interrupted in S1, where temperatures decreases by 4.7 °C and relative to the YD (19.9 °C). Modern SST_{TEX86} is not reached before 4.7 kyr BP.

SST_{TEX} suggests an LGM to late Holocene warming of ca. 18 °C, ca. 8 °C larger than for the Mediterranean Sea (Castañeda et al., 2010) and Black Sea (Ménot and Bard, 2010). SST_{LDI} suggests a LGM to Holocene warming of 13 °C on average, but the maximum amplitude is almost 20 °C between 6.96 kyr BP and the LGM (21.29 kyr BP). The $SST_{UK'37}$ difference between the youngest Holocene and the YD is ca. 14 °C and in good agreement with other $SST_{UK'37}$ records from the Sea of Marmara (Sperling et al., 2003; Ménot and Bard, 2010; Vidal et al., 2010). Our $SST_{UK'37}$ record is closely similar to that of Sperling et al. (2003) for the time interval where both records overlap (YD to modern Holocene). This supports the novel protocol. There is an offset of ca. 2 °C between the two records during the Holocene. Sperling et al. (2003) determined $SST_{UK'37}$ from the total lipid extract without removing coeluting alkenoates, which may explain the offset. The novel MS-based protocol circumvents such potential bias caused by elevated levels of alkenoates. Other potential explanations are the slightly different core locations or differences in instrument performance. It has for example been shown in an interlaboratory study that absolute values can differ by up to 2 °C for exactly the same sample (Rosell-Melé et al., 2001).

The high $SST_{UK'37}$ values during the last glacial are unrealistic and indicate that the transfer function is not valid for the lacustrine setting in the Sea of Marmara during that time. In lacustrine settings, alkenone-producing taxa occur with $U^{K'}_{37}$-SST relationships very different from that of *E. huxleyi* (e.g. Versteegh et al., 2001; Zink et al., 2001; Toney et al., 2010). Coccolith analysis shows that *E. huxleyi* was only abundant during the marine phase (0–14.7 kyr BP) but not during the lacustrine phase (14.7–21 kyr BP), when overall abundance and diversity of coccoliths was low (Aksu et al., 2002).

The change in coccolith species coincides with a change in salinity, which was low during the last glacial and increased after the marine connection in the Sea of Marmara was established (e.g. Sperling et al., 2003; Vidal et al., 2010). *E. huxleyi* likely "invaded" the Sea of Marmara after this flooding by Mediterranean water during deglaciation, as also suggested for the Black Sea (Hay et al., 1991). Our $SST_{UK'37}$ record, as well as evidence for hydrological and ecological changes (e.g. Aksu et al., 1999, 2002; Sperling et al., 2003; Vidal et al., 2010), strongly suggests that SST reconstruction based on alkenones is not suitable for the lacustrine phase in the Sea of Marmara using the current transfer function.

In contrast, SST_{LDI} and SST_{TEX86} are low during the last glacial and, as expected, show warming at the transition to the B/A. Clearly, the ecological and hydrological changes in the Sea of Marmara had less influence on the relationship between temperature and the distributions of *i*GDGTs and long chain diols. This is in agreement with mesocosm incubations of enriched *Thaumarchaeota* under different salinity conditions (Wuchter et al., 2004). In S1, a significant cooling of ca. 5 °C occurs in SST_{TEX86}. Cooling during sapropel formation based on TEX_{86} has also been reported for Pliocene sapropels from the Black Sea (Menzel et al., 2006). This observation has been explained by a strong contribution from marine Crenarchaeota, thriving at the deeper and colder chemocline. At the time of the sapropel formation in the Sea of Marmara, a similar effect could have led to a change in the distribution of *i*GDGTs. A chemocline could have developed as a result of higher primary productivity and reduced mixing of the water masses, leading to O_2 depletion and bottom water anoxia (e.g. Sperling et al., 2003; Vidal et al., 2010). Therefore, *Thaumarchaeota* could have been driven to a different ecological niche. In modern nutrient-replete nearshore and oceanic upwelling environments, such a cold bias has also been observed (Huguet et al., 2007; Lee et al., 2008; Leider et al., 2010; Wei et al., 2011) and been interpreted as a shift in the depth of GDGT production (Kim et al., 2008; Taylor et al., 2013). However, these interpretations have to be revised since more recent studies showed a bias towards higher TEX_{86} temperature estimates for subsurface waters (Schouten et al., 2012; Basse et al., 2014; Hernández-Sánchez et al., 2014; Xie et al., 2014), which indicates a distinct relationship between *i*GDGT biosynthesis and temperature from subsurface archaea. The influence of physiology and environment on TEX_{86}in cultures of marine planktonic *Thaumarchaeota* has not been systematically studied. The only exception is a study of *Nitrosopumilus maritimus* (Elling et al., 2014), where the *i*GDGT distribution, and conversely TEX_{86}, changed with growth phase, independent of temperature. One trigger for the sapropel formation in the Sea of Marmara is enhanced primary productivity due to the inflow of Mediterranean water (Sperling et al., 2003; Vidal et al., 2010), also suggesting increased nutrient influx. Such a change in nutrient availability could have changed the *i*GDGT-temperature relationship (cf. Turich et al., 2007; Elling et al., 2014), but further studies are needed to assess the impact of factors other than temperature influencing *i*GDGT distribution.

The expected warming during the B/A and the cooling during the YD are not reflected in any of the SST records. This has also been observed by others using $U^{K'}_{37}$ in the Sea of Marmara (Sperling et al., 2003; Vidal et al., 2010). Sperling et al. (2003) argued that warmer water originating from the Mediterranean Sea or the incorporation of 'old' alkenones from the preceding B/A interstadial might have distorted the temperature signal. This is in contrast to records from the western (Rodrigo-Gámiz et al., 2014) and Eastern Mediterranean Sea (Castañeda et al., 2010), where climate change during the YD and the B/A was documented by the (SS)T proxies. In our case, the limited number of samples at the transitions of the different climatic events might explain why the changes were not observed.

The incongruent changes of $SST_{UK'37}$ and SST_{LDI} from the B/A to the termination of S1 further suggest that other environmental factors such as nutrient availability, salinity and O_2 availability affected the proxy temperature relationship for diols and alkenones. For example, beside changes in species composition that can lead to erroneous $U^{K'}_{37}$ temperature reconstruction (see above), culture experiments with different haptophytes revealed the alteration of the alkenone distribution with changing light intensity, cell division rate, salinity and nutrient concentration (Epstein et al., 1998; Versteegh et al., 2001; Prahl et al., 2003; Ono et al., 2012). Accordingly, the environmental changes that occurred in the Sea of Marmara since the last glacial (e.g. Vidal et al., 2010) have potentially impacted the alkenone distribution in addition to changes in temperature. The mechanism behind the correlation between LDI and temperature, the exact biological source and the effect of environmental factors on the LDI needs to be constrained (cf. Rampen et al., 2012), but adaptation in lipid composition to multiple environmental variables can be expected for most organisms (e.g. Hazel and Williams, 1990).

The differences in absolute temperature between the three proxies, particularly for the Holocene, might be explained by differences in the growing season of the source species (e.g. Leider et al., 2010; Castañeda et al., 2010; Lopes dos Santos et al., 2013; Rodrigo-Gámiz et al., 2014). However, absolute temperatures have to be interpreted with caution, since the differences could simply be within the uncertainties in the temperature calibrations for the individual proxies. As a complementary approach to the global core-top calibration to convert TEX_{86} to temperature, we used the BAYSPAR calibration model (Fig. S2), which produces meaningful uncertainty estimates (Tierney and Tingley, 2014). We applied the "standard prediction" mode and used the default settings. The SST estimates based on this calibration showed the same trend as those obtained from the global core-top calibration, but absolute values were consistently lower (between 1.3 and 4 °C). The 90% uncertainty intervals (Fig. S2, light blue area) extend about 10 °C for a single sample. Considering additionally the standard errors for the calibrations of the other two SST proxies, which do not fully account for uncertainties, it becomes apparent that speculation on absolute temperature differences is problematic.

4. Conclusions

For reconstructing climate and environment, reliable and rapid assessment of past temperature is essential. We have demonstrated a rapid and reliable method for determination of the lipid based $U^{K'}_{37}$, LDI and TEX_{86} temperature proxies within a single NP-HPLC–MS analysis. The method permits the direct analysis of TLEs, saving time-consuming and error-prone cleanup procedures. The reduction in analytical processing time is at least one day for eliminating the saponification, derivatization and fractionation steps, whereas the measurement time is reduced to 60 min/sample for all the compounds for the NP-HPLC–APCI-MS method. $U^{K'}_{37}$ values obtained with HPLC–MS and GC-FID, as well as LDI values obtained with HPLC–MS and GC–MS, were similar and showed almost a 1:1 linear relationship. To monitor the stability of the method and to further assess the validity of a correction function, the use of reference samples is recommended, for $U^{K'}_{37}$ preferably based on pure alkenone standards with known $U^{K'}_{37}$ values. The application of the new method to a sediment core from the Sea of Marmara was in agreement with literature data on lipid based paleo SST proxies from the region. The discrepancies between the SST proxies in the sediment record likely derive from parameters other than temperature affecting the distributions of the relevant lipids. However, the different ecologies of the organisms are poorly understood. In particular, more insight into the physiological responses of the organisms to a changing environment and their effects on the proxies are needed.

The proposed NP-HPLC–APCI-MS protocol allows determination of nine paleoenvironmental proxies within a single analysis. Since in most modern organic chemical laboratories HPLC systems are available, the protocol could be established for routinely use as a tool for environmental reconstruction.

Acknowledgements

We thank the crew, chief scientist, M. Zabel, and the scientific shipboard party of the RV Meteor cruise M84/1 (DARCSEAS I). We further thank I.D. Bull for providing alkenone standards, R. Himmelsbach for growing *E. huxleyi*, S. Alfken, C. Vogel and T. Stoltmann for help with sample preparation for lipid analysis and lipid quantification, and F. Schmidt and M. Elvert for stimulating discussions. We would also like to thank M.A. Lever, H. Røy and B.B. Jørgensen from the Center for Geomicrobiology at Aarhus University, and the crew of Aarhus University's research vessel Tyra, for support in the sampling and processing of Aarhus Bay sediment samples. The study was funded by the European Research Council under the European Union's Seventh Framework Programme – "Ideas" Specific Programme, ERC grant agreement # 247153 (Advanced Grant DARCLIFE; PI K.-U.H.) and by the Deutsche Forschungsgemeinschaft (DFG, Germany) through grants Inst 144/300-1 (LC-qToF system), VE486/3 (G.J.M.V.). Further support was given by the Bremen International Graduate School for Marine Sciences (GLOMAR) funded by the DFG through MARUM Center for Marine Environmental Sciences. We thank J.E. Tierney and an anonymous reviewer for constructive comments and suggestions.

Appendix A. Supplementary data

Supplementary data associated with this article can be found, in the online version, at http://dx.doi.org/10.1016/j.orggeochem.2015.04.008.

Associate Editor—**S. Derenne**

References

Aksu, A.E., Hiscott, R.N., Yaşar, D., 1999. Oscillating Quaternary water levels of the Marmara Sea and vigorous outflow into the Aegean Sea from the Marmara Sea-Black Sea drainage corridor. Marine Geology 153, 275–302.

Aksu, A.E., Hiscott, R.N., Mudie, P.J., Rochon, A., Kaminski, M.A., Abrajano, T., Yasar, D., 2002. Persistent Holocene outflow from the Black Sea to the eastern Mediterranean contradicts Noah's flood hypothesis. GSA Today 12, 4–10.

Basse, A., Zhu, C., Versteegh, G.J.M., Fischer, G., Hinrichs, K.-U., Mollenhauer, G., 2014. Distribution of intact and core tetraether lipids in water column profiles of suspended particulate matter off Cape Blanc, NW Africa. Organic Geochemistry 72, 1–13.

Becker, K.W., Lipp, J.S., Zhu, C., Liu, X.L., Hinrichs, K.-U., 2013. An improved analytical method for the analysis of archaeal and bacterial ether lipids. Organic Geochemistry 61, 34–44.

Brassell, S.C., Eglinton, G., Marlowe, I.T., Pflaumann, U., Sarntheim, M., 1986. Molecular stratigraphy: a new tool for climatic assessment. Nature 320, 129–133.

Chaler, R., Grimalt, J.O., Pelejero, C., Calvo, E., 2000. Sensitivity effects in $U^{K'}_{37}$ paleotemperature estimation by chemical ionization mass spectrometry. Analytical Chemistry 72, 5892–5897.

Çağatay, N.M.O., Sakinç, M., Eastoe, C., Egesel, L., Balkis, N., Ongan, D., Caner, H., 1999. A mid-late Holocene sapropelic sediment unit from the southern Marmara shelf and its paleoceanographic significance. Quaternary Science Reviews 18, 531–540.

Çağatay, M.N., Görür, N., Algan, O., Eastoe, C., Tchapalyga, A., Ongan, D., Kuhn, T., Kuşçu, I., 2000. Late Glacial-Holocene palaeoceanography of the Sea of Marmara: timing of connections with the Mediterranean and the Black Seas. Marine Geology 167, 191–206.

Castañeda, I.S., Schefuß, E., Pätzold, J., Sinninghe Damsté, J.S., Weldeab, S., Schouten, S., 2010. Millennial-scale sea surface temperature changes in the eastern Mediterranean (Nile River Delta region) over the last 27,000 years. Paleoceanography 25, PA1208. http://dx.doi.org/10.1029/2009PA001740.

Chaler, R., Villanueva, J., Grimalt, J.O., 2003. Non-linear effects in the determination of paleotemperature $U^{K'}_{37}$ alkenone ratios by chemical ionization mass spectrometry. Journal of Chromatography A 1012, 87–93.

Conte, M.H., Sicre, M.-A., Rühlemann, C., Weber, J.C., Schulte, S., Schulz-Bull, D., Blanz, T., 2006. Global temperature calibration of the alkenone unsaturation index ($U^{K'}_{37}$) in surface waters and comparison with surface sediments. Geochemistry Geophysics Geosystems 7, Q02005. http://dx.doi.org/10.1029/2005GC001054.

Elling, F.J., Könneke, M., Lipp, J.S., Becker, K.W., Gagen, E.J., Hinrichs, K.-U., 2014. Effects of growth phase on the membrane lipid composition of the thaumarchaeon Nitrosopumilus maritimus and their implications for archaeal lipid distributions in the marine environment. Geochimica et Cosmochimica Acta 141, 579–597.

Elvert, M., Boetius, A., Knittel, K., Jørgensen, B.B., 2003. Characterization of specific membrane fatty acids as chemotaxonomic markers for sulfate-reducing bacteria involved in anaerobic oxidation of methane. Geomicrobiology Journal 20, 403–419.

Epstein, B.L., D'Hondt, S., Quinn, J.G., Zhang, J., Hargraves, P.E., 1998. An effect of dissolved nutrient concentrations on alkenone-based temperature estimates. Paleoceanography 13, 122–126.

Grauel, A.-L., Leider, A., Goudeau, M.-L.S., Müller, I.A., Bernasconi, S.M., Hinrichs, K.-U., De Lange, G.J., Zonneveld, K.A.F., Versteegh, G.J.M., 2013. What do SST proxies really tell us? A high-resolution multiproxy ($U^{K'}_{37}$, $TEXH_{86}$ and foraminifera $\delta^{18}O$) study in the Gulf of Taranto, central Mediterranean Sea. Quaternary Science Reviews 73, 115–131.

Grimalt, J.O., Calvo, E., Pelejero, C., 2001. Sea surface paleotemperature errors in $U^{K'}_{37}$ estimation due to alkenone measurements near the limit of detection. Paleoceanography 16, 226–232.

Guillard, R.R.L., Ryther, J.H., 1962. Studies of marine planktonic diatoms. I. *Cyclothella nana* (Hustedt) and *Detonulaconfervacea* (Cleve). Canadian Journal of Microbiology 8, 229–239.

Hefter, J., 2008. Analysis of alkenone unsaturation indices with fast gas chromatography/time-of-flight mass spectrometry. Analytical Chemistry 80, 2161–2170.

Hay, B.J., Arthur, M.A., Dean, W.E., Neff, E.D., Honjo, S., 1991. Sediment deposition in the Late Holocene abyssal Black Sea with climatic and chronological implications. Deep-Sea Research 38, 1211–1235.

Hazel, J.R., Williams, E.E., 1990. The role of alterations in membrane lipid composition in enabling physiological adaptation of organisms to their physical environment. Progress in Lipid Research 29, 167–227.

Herbert, T.D., 2003. Alkenone paleotemperature determinations. In: Holland, H.D., Turekian, K.K. (Eds.), The Ocean and Marine Geochemistry. Treatise on Geochemistry, vol. 6. Elsevier Pergamon, Oxford, pp. 365–390.

Hernández-Sánchez, M.T., Woodward, E.M.S., Taylor, K.W.R., Henderson, G., Pancost, R.D., 2014. Variations in GDGT distributions through the water column in the South East Atlantic Ocean. Geochimica et Cosmochimica Acta 132, 337–348.

Hoefs, M.J.L., Versteegh, G.J.M., de Leeuw, J.W., Sinninghe Damsté, J.S., 1998. Postdepositional oxic degradation of alkenones: implications for the measurement of paleo sea surface temperatures. Paleoceanography 13, 42–49.

Hopmans, E.C., Schouten, S., Pancost, R.D., Van der Meer, M.T.J., Sinninghe Damsté, J.S., 2000. Analysis of intact tetraether lipids in archaeal cell material and sediments by high performance liquid chromatography/atmospheric pressure chemical ionization mass spectrometry. Rapid Communications in Mass Spectrometry 14, 585–589.

Hopmans, E.C., Weijers, J.W.H., Schefuß, E., Herfort, L., Sinninghe Damsté, J.S., Schouten, S., 2004. A novel proxy for terrestrial organic matter in sediments based on branched and isoprenoid tetraether lipids. Earth and Planetary Science Letters 224, 107–116.

Huguet, C., Hopmans, E.C., Febo-Ayala, W., Thompson, D.H., Sinninghe Damsté, J.S., Schouten, S., 2006. An improved method to determine the absolute abundance of glycerol dibiphytanyl glycerol tetraether lipids. Organic Geochemistry 37, 1036–1041.

Huguet, C., Schimmelmann, A., Thunell, R., Lourens, L.J., Sinninghe Damsté, J.S., Schouten, S., 2007. A Study of the TEX_{86} paleothermometer in the water column and sediments of the Santa Barbara Basin, California. Paleoceanography 22, PA3203.

Huguet, C., Kim, J.-H., de Lange, G.J., Sinninghe Damsté, J.S., Schouten, S., 2009. Effects of long term oxic degradation on the $U^{K'}_{37}$, TEX_{86} and BIT organic proxies. Organic Geochemistry 40, 1188–1194.

Huguet, C., Fietz, S., Rosell-Melé, A., 2013. Global distribution patterns of hydroxy glycerol dialkyl glycerol tetraethers. Organic Geochemistry 57, 107–118.

Kim, J.-H., Schouten, S., Hopmans, E.C., Donner, B., Sinninghe Damsté, J.S., 2008. Global core-top calibration of the TEX_{86} paleothermometer in the ocean. Geochimica et Cosmochimica Acta 72, 1154–1173.

Kim, J.-H., Crosta, X., Michel, E., Schouten, S., Duprat, J., Sinninghe Damsté, J.S., 2009. Impact of lateral transport on organic proxies in the Southern Ocean. Quaternary Research 71, 246–250.

Lee, K.E., Kim, J.-H., Wilke, I., Helmke, P., Schouten, S., 2008. A study of the alkenone, TEX_{86}, and planktonic foraminifera in the Benguela Upwelling System: implications for past sea surface temperature estimates. Geochemistry, Geophysics, Geosystems 9, Q10019.

Leider, A., Hinrichs, K.-U., Mollenhauer, G., Versteegh, G.J.M., 2010. Core-top calibration of the lipid-based $U^{K'}_{37}$ and TEX_{86} temperature proxies on the southern Italian shelf (SW Adriatic Sea, Gulf of Taranto). Earth and Planetary Science Letters 300, 112–124.

Liu, X.-L., Summons, R.E., Hinrichs, K.-U., 2012. Extending the known range of glycerol ether lipids in the environment: structural assignments based on MS/MS fragmentation patterns. Rapid Communications in Mass Spectrometry 26, 2295–2302.

Lopes dos Santos, R.A., Spooner, M.I., Barrows, T.T., De Deckker, P., Sinninghe Damsté, J.S., Schouten, S., 2013. Comparison of organic ($U^{K'}_{37}$, TEX^{H}_{86}, LDI) and faunal proxies (foraminiferal assemblages) for reconstruction of late Quaternary sea-surface temperature variability from offshore southeastern Australia. Paleoceanography 28, 377–387.

López, J.F., Grimalt, J.O., 2004. Phenyl- and cyclopentylimino derivatization for double bond location in unsaturated C_{37}–C_{40} alkenones by GC–MS. Journal of the American Society for Mass Spectrometry 15, 1161–1172.

Ménot, G., Bard, E., 2010. Geochemical evidence for a large methane release during the last deglaciation from Marmara Sea sediments. Geochimica Cosmochimica Acta 74, 1537–1550.

Menzel, D., Hopmans, E.C., Schouten, S., Sinninghe Damsté, J.S., 2006. Membrane tetraether lipids of planktonic Crenarchaeota in Pliocene sapropels of the eastern Mediterranean Sea. Palaeogeography, Palaeoclimatology, Palaeoecology 239, 1–15.

Mollenhauer, G., Eglinton, T.I., Ohkouchi, N., Schneider, R.R., Müller, P.J., Grootes, P.M., Rullkötter, J., 2003. Asynchronous alkenone and foraminifera records from the Benguela Upwelling System. Geochimica et Cosmochimica Acta 67, 2157–2171.

Müller, P.J., Kirst, G., Ruhland, G., von Storch, I., Rosell-Melé, A., 1998. Calibration of the alkenone paleotemperature index $U^{K'}_{37}$ based on core-tops from the eastern South Atlantic and the global ocean (60°N–60°S). Geochimica et Cosmochimica Acta 62, 1757–1772.

Nichols, P.D., Shaw, P.M., Mancuso, C.A., Franzmann, P.D., 1993. Analysis of archaeal phospholipid-derived diether and tetraether lipids by high-temperature capillary gas-chromatography. Journal of Microbiological Methods 18, 1–9.

Ohkouchi, N., Eglinton, T.I., Keigwin, L.D., Hayes, J.M., 2002. Spatial and temporal offsets between proxy records in a sediment drift. Science 298, 1224–1227.

Ono, M., Sawada, K., Shiraiwa, Y., Kubota, M., 2012. Changes in alkenone and alkenoate distributions during acclimatization to salinity change in *Isochrysis galbana*: implication for alkenone-based paleosalinity and paleothermometry. Geochemical Journal 46, 235–247.

Pancost, R.D., Coleman, J.M., Love, G.D., Chatzi, A., Bouloubassi, I., Snape, C.E., 2008. Kerogen-bound glycerol dialkyl tetraether lipids released by hydropyrolysis of marine sediments: a bias against incorporation of sedimentary organisms? Organic Geochemistry 39, 1359–1371.

Prahl, F.G., Wakeham, S.G., 1987. Calibration of unsaturation patterns in long-chain ketone compositions for paleotemperature assessment. Nature 330, 367–369.

Prahl, F.G., Muehlhausen, L.A., Zahnle, D.L., 1988. Further evaluation of long-chain alkenones as indicators of paleoceanographic conditions. Geochimica et Cosmochimica Acta 52, 2303–2310.

Prahl, F.G., Wolfe, G.V., Sparrow, M.A., 2003. Physiological impacts on alkenone paleothermometry. Paleoceanography 18. http://dx.doi.org/10.1029/2002PA000803.

Rampen, S.W., Willmott, V., Kim, J.-Y., Uliana, E., Mollenhauer, G., Schefuß, E., Sinninghe Damsté, J.S., Schouten, S., 2012. Long chain 1,13- and 1,15-diols as a potential proxy for palaeotemperature reconstruction. Geochimica et Cosmochimica Acta 84, 204–216.

Rodrigo-Gámiz, M., Martínez-Ruiz, F., Rampen, S.W., Schouten, S., Sinninghe Damsté, J.S., 2014. Sea surface temperature variations in the western Mediterranean Sea over the last 20 kry: a dual-organic proxy ($U^{K'}_{37}$ and LDI) approach. Paleoceanography 29, 87–98.

Rontani, J.-F., Prahl, F.G., Volkman, J.K., 2006. Characterization of unusual alkenones and alkyl alkenoates by electron ionization gas chromatography/mass spectrometry. Rapid Communications in Mass Spectrometry 20, 583–588.

Rosell-Melé, A., Carter, J.F., Parry, A.T., Eglinton, G., 1995. Determination of the U^{K}_{37} index in geological samples. Analytical Chemistry 67, 1283–1289.

Rosell-Melé, A. et al., 2001. Precision of the current methods to measure the alkenone proxy $U^{K'}_{37}$ and absolute alkenone abundance in sediments: results of an interlaboratory comparison study. Geochemistry, Geophysics, Geosystems 2, 1046. http://dx.doi.org/10.1029/2000GC000141.

Ryan, W.B.F., Pitman, W.C., Major, C.O., Shimkus, K., Moskalenko, V., Jones, G.A., Dimitrov, P., Görür, N., Sakinç, M., Yüce, H., 1997. An abrupt drowning of the Black Sea shelf. Marine Geology 138, 119–126.

Ryan, W.B.F., Major, C.O., Lericolais, G., Goldstein, S.L., 2003. Catastrophic flooding of the Black Sea. Annual Review of Earth and Planetary Sciences 31, 525–554.

Schouten, S., Hopmans, E.C., Schefuß, E., Sinninghe Damsté, J.S., 2002. Distributional variations in marine crenarchaeotal membrane lipids: a new tool for reconstructing ancient sea water temperatures? Earth and Planetary Science Letters 204, 265–274.

Schouten, S., Hopmans, E.C., Sinninghe Damsté, J.S., 2004. The effect of maturity and depositional redox conditions on archaeal tetraether lipid paleothermometry. Organic Geochemistry 35, 567–571.

Schouten, S., Huguet, C., Hopmans, E.C., Sinninghe Damsté, J.S., 2007. Improved analytical methodology of the TEX_{86} paleothermometry by high performance liquid chromatography/atmospheric pressure chemical ionization-mass spectrometry. Analytical Chemistry 79, 2940–2944.

Schouten, S., Pitcher, A., Hopmans, E.C., Villanueva, L., van Bleijswijk, J., Sinninghe Damsté, J.S., 2012. Intact polar and core glycerol dibiphytanyl glycerol tetraether lipids in the Arabian Sea oxygen minimum zone: I. Selective preservation and degradation in the water column and consequences for the TEX_{86}. Geochimica et Cosmochimica Acta 98, 228–243.

Schulz, H.M., Schoner, A., Emeis, K.C., 2000. Long-chain alkenone patterns in the Baltic Sea - an ocean-freshwater transition. Geochimica et Cosmochimica Acta 64, 469–477.

Smith, D.J., Eglinton, G., Morris, R.J., 1983. Occurrence of long-chain alkane-diols and alkan-15-one-1-ols in a Quaternary sapropel from the Eastern Mediterranean. Lipids 18, 902–905.

Smith, M., De Deckker, P., Rogers, J., Brocks, J., Hope, J., Schmidt, S., Lopes dos Santos, R., Schouten, S., 2013. Comparison of $U^{K'}_{37}$, TEX_{86} and LDI temperature proxies for reconstruction of south-east Australian ocean temperatures. Organic Geochemistry 64, 94–104.

Sperling, M., Schmiedl, G., Hembleben, Ch., Emeis, K.C., Erlenkeuser, H., Grootes, P.M., 2003. Black Sea impact on the formation of eastern Mediterranean sapropel S1? Evidence from the Marmara Sea. Palaeogeography, Palaeoclimatology, Palaeoecology 190, 9–21.

Stanley, D.J., Blanpied, C., 1980. Late Quaternary water exchange between the eastern Mediterranean and the Black Sea. Nature 266, 537–541.

Sturt, H.F., Summons, R.E., Smith, K., Elvert, M., Hinrichs, K.-U., 2004. Intact polar membrane lipids in prokaryotes and sediments deciphered by high-performance liquid chromatography/electrospray ionization multistage mass spectrometry: new biomarkers for biogeochemistry and microbial ecology. Rapid Communications in Mass Spectrometry 18, 617–628.

Taylor, K.W.R., Huber, M., Hollis, C.J., Hernández-Sánchez, M.T., Pancost, R.D., 2013. Re-evaluating modern and Paleogene GDGT distributions: implications for SST reconstructions. Global and Planetary Change 108, 158–174.

Thiel, V., Jenisch, A., Landmann, G., Reimer, A., Michaelis, W., 1997. Unusual distributions of long-chain alkenones and tetrahymanol from the highly alkaline Lake Van, Turkey. Geochimica et Cosmochimica Acta 61, 2053–2064.

Tierney, J.E., Tingley, M.P., 2014. A Bayesian, spatially-varying calibration model for the TEX_{86} proxy. Geochimica et Cosmochimica Acta 127, 83–106.

Toney, J.L., Huang, Y., Fritz, S.C., Baker, P.A., Grimm, E., Nyren, P., 2010. Climatic and environmental controls on the occurrence and distributions of long chain alkenones in lakes of the interior United States. Geochimica et Cosmochimica Acta 74, 1563–1578.

Turich, C., Freeman, K.H., Bruns, M.A., Conte, M., Jones, A.D., Wakeham, S.G., 2007. Lipids of marine archaea: patterns and provenance in the water-column and sediments. Geochimica et Cosmochimica Acta 71, 3272–3291.

Turich, C., Freeman, K.H., 2011. Archaeal lipids record paleosalinity in hypersaline systems. Organic Geochemistry 42, 1147–1157.

Versteegh, G.J.M., Bosch, H.-J., de Leeuw, J.W., 1997. Potential paleoenvironmental information of C_{24} to C_{36} mid-chain diols, keto-ols and mid-chain hydroxy fatty acids; a critical review. Organic Geochemistry 27, 1–13.

Versteegh, G.J.M., Riegman, R., de Leeuw, J.W., Jansen, J.H.F., 2001. $U^{K'}_{37}$ values for *Isochrysis galbana* as a function of culture temperature, light intensity and nutrient concentrations. Organic Geochemistry 32, 785–794.

Vidal, L., Ménot, G., Joly, C., Bruneton, H., Rostek, F., Çağatay, M.N., Major, C., Bard, E., 2010. Hydrology in the Sea of Marmara during the last 23 ka: implications for timing of Black Sea connections and sapropel deposition. Paleoceanography 25, PA1205.

Villanueva, J., Pelejero, C., Grimalt, J.O., 1997. Clean-up procedures for the unbiased estimation of C_{37} alkenone sea surface temperatures and terrigenous *n*-alkane inputs in paleoceanography. Journal of Chromatography A 757, 145–151.

Villanueva, J., Grimalt, J.O., 1997. Gas chromatographic tuning of the $U^{K'}_{37}$ paleothermometer. Analytical Chemistry 69, 3329–3332.

Volkman, J.K., Barrett, S.M., Dunstan, G.A., Jeffrey, S.W., 1992. C_{30}–C_{32} alkyl diols and unsaturated alcohols in microalgae of the class Eustigmatophyceae. Organic Geochemistry 18, 131–138.

Wei, Y., Wang, J., Liu, J., Dong, L., Li, L., Wang, H., Wang, P., Zhao, M., Zhang, C.L., 2011. Spatial variations in archaeal lipids of surface water and core-top sediments in the South China Sea and their implications for paleoclimate studies. Applied and Environmental Microbiology 77, 7479–7489.

Weijers, J.W.H., Schouten, S., van den Donker, J.C., Hopmans, E.C., Sinninghe Damsté, J.S., 2007. Environmental controls on bacterial tetraether membrane lipid distribution in soils. Geochimica et Cosmochimica Acta 71, 703–713.

Wuchter, C., Schouten, S., Coolen, M.J.L., Sinninghe Damsté, J.S., 2004. Temperature dependent variation in the distribution of tetraether membrane lipids of marine Crenarchaeota: implications for TEX_{86} paleothermometry. Paleoceanography 19, PA4028.

Xie, S., Liu, X.-L., Schubotz, F., Wakeham, S.G., Hinrichs, K.-U., 2014. Distribution of glycerol ether lipids in the oxygen minimum zone of the Eastern Tropical North Pacific Ocean. Organic Geochemistry 71, 60–71.

Zabel, M. and cruise participants, 2011. RV METEOR, Cruise Report M84/L1, Biogeochemistry and Methane Hydrates of the Black Sea; Oceanography of the Mediterranean; Shelf Sedimentation and cold water carbonates 2011. DFG Senatskommission für Ozeanographie, 39 pp. http://dx.doi.org/10.2312/cr_m84_1.

Zhang, Y.G., Zhang, C.L., Liu, X.-L., Hinrichs, K.-U., Noakes, J.E., 2011. Methane index: a tetraether archaeal lipid biomarker indicator for detecting the instability of marine gas hydrates. Earth and Planetary Science Letters 307, 525–534.

Zhu, C., Lipp, J.S., Wörmer, L., Becker, K.W., Schröder, J., Hinrichs, K.-U., 2013. Comprehensive glycerol ether lipid fingerprints through a novel reverse-phase liquid chromatography-mass spectrometry protocol. Organic Geochemistry 65, 53–62.

Zhu, C., Meador, T.B., Dummann, W., Hinrichs, K.-U., 2014. Identification of unusual butanetriol dialkyl glycerol tetraether and pentanetriol dialkyl glycerol tetraether lipids in marine sediments. Rapid Communications in Mass Spectrometry 28, 332–338.

Zink, K.G., Leythaeuser, D., Melkonian, M., Schwark, L., 2001. Temperature dependency of long-chain alkenone distributions in recent to fossil limnic sediments and in lake waters. Geochimica et Cosmochimica Acta 65, 253–265.